ACS APPLIED MATERIALS & INTERFACES

Research Article

www.acsami.org

Two-Dimensional Periodic Relief Grating as a Versatile Platform for Selective Immunosorbent Assay and Visualizing of Antigens

Jem-Kun Chen,*[,†] Gang-Yan Zhou,[†] Chih-Feng Huang,[‡] and Jia-Yaw Chang[§]

[†]Department of Materials Science and Engineering, National Taiwan University of Science and Technology, 43, Sec. 4, Keelung Road, Taipei, 106, Taiwan, Republic of China

[‡]Department of Chemical Engineering, National Chung Hsing University, Eng Bld 3, 250 Kuo Kuang Road, 402 Taichung, Taiwan

[§]Department of Chemical Engineering, National Taiwan University of Science and Technology, 43, Sec. 4, Keelung Road, Taipei, 106, Taiwan, Republic of China

ABSTRACT: In this study, we fabricated a nanopillar array of silicon oxide, involving very-large-scale integration (VLSI) and reactive ion etching (RIE), as two-dimensional periodic relief gratings (2DPRGs) on Si surfaces. Antihuman ALB was successively oriented on the pillar surface of 2DPRG modified protein G as an optical detector that is specific for targeted antigen. The antibody modified 2DPRG alone produces insignificant structure change, but upon immunocapture of antigens, the antigen filling in the 2DPRG leads to a dramatic change of the pillar scale. Binding of the antibodies to the 2DPRG occurs in a way that still allows them to function and selectively bind antigen. The performance of the sensor was evaluated by capturing HRP-human ALB on the antibody-modified 2DPRG and measuring the effective refractive index (n_{eff}) resulting from the attachment of antigens. The n_{eff} values of the 2DPRG are found to relate with the pillar scale of the 2DPRG, generated by antigen coupling, resulting in color change from pure green to orange, observed by the naked eye along an incident angle of 10−20°. Moreover, we calculated the filling factors inside the 2DPRG with effective-medium theory to verify the pillar structure changes. This technique eliminates much of the surface modifications and the secondary immunochemical or enzyme-linked steps that are common in immunoassays. Such films have potential applications as optical biosensors.

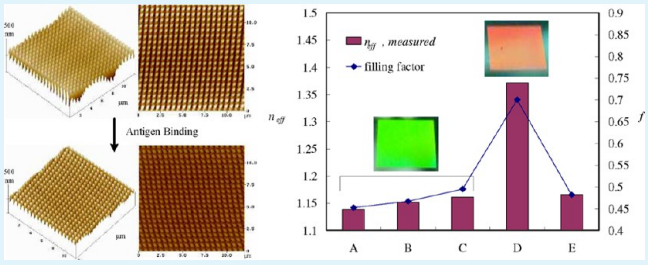

KEYWORDS: *two-dimensional periodic grating, refractive index, effective medium theory, immunoassay*

INTRODUCTION

Detection of proteins in a sensitive and rapid manner plays an essential role in clinical applications. Numerous studies have been reported on using antibody-based immunoassay systems as recognition elements for detecting proteins.[1−3] Among many other biosensing platforms, the effectiveness of optical diffraction based biosensors has been demonstrated for recognizing binding events of various biomolecules, which operate based on changes in effective height or refractive index on periodically patterned gratings.[4,5] Antibodies are generally produced in vivo, which have been used as recognition elements in a number of biosensing platforms.[6,7] However, even though antibodies uniquely transduce the recognition of antigen into the generation of readily observable signals, antigens in small quantities are still difficult to detect with antibody alone, pointing to a need for novel signal enhancement schemes.

Recently, a number of different types of optical biological sensors have been reported that involve the measurement of diffraction patterns as assay readout. Alternatively, optical detection methods can employ surface plasmon resonance,[8,9] surface acoustic waves,[10] and fiber optical techniques.[11] The use of optical diffraction as a means to detect complex formation on a silicon wafer was applied to the detection of choriogonadotropin in serum samples.[12] The sensor described in this earlier paper, however, required a surface coated with an antibody that is then deactivated by ultraviolet light through a mask to generate the pattern. Reproducibility in the antibody inactivation and in the scale-up of fabrication would be problems with this approach. Moreover, because protein layers are ultrathin, heterogeneous, and heavily mixed with water, the change in refractive index across the interface arising from protein adsorption is small. Techniques such as optical reflectometry, surface plasmon resonance (SPR), and ellipsometry base their measurements on detecting the change of refractive index, and although they are able to provide useful estimates of the adsorbed amount, they have little inherent sensitivity to layer thickness and composition.[13,14]

Subwavelength structured (SWS) surfaces are attractive for new optical elements, and many different elements with these surfaces have been developed. A mean refractive index can be controlled by the filling factors of the structure, so that a desired distribution of refractive index can be realized. Well-arranged SWS surfaces also behave like artificial dielectrics,

Received: January 30, 2013
Accepted: March 19, 2013
Published: March 19, 2013

   dx.doi.org/10.1021/am4004123 | *ACS Appl. Mater. Interfaces* 2013, 5, 3348−3355

where the isotropic and anisotropic materials can be synthesized. By careful design of the SWS structure, a high efficiency diffraction grating can be synthesized even with the binary profile. When the SWS element is a 1D periodic surface or an unsymmetrical 2D periodic surface, the effective refractive index depends upon polarization states of the incident light. A nanopillar (NPL) array is one kind of SWS surface, a symmetrical 2D periodic surface, currently attracting a great interest due to their potential applications in grating or photonics.[15] The term nanopillar (NPL) usually refers to an elongated object of diameter in the 150−500 nm range standing perpendicularly to the substrate.[16] NPLs have unique optical properties due to their one-dimensional geometry, including polarized photoresponse, diameter tunable band structure, and biosensing.[17−19] When the NPLs interact specifically or nonspecifically with target molecules, the geometrical parameters of the gratings and/or the refractive index contrast typically change.[20]

In many studies, in order to detect small amounts of biomolecules, additional signal enhancement was necessary.[21] The enhancement was accomplished either by microfabrication of solid diffraction gratings or by in situ assembled diffraction gratings that are self-fabricated by nano- or microsize particles. In comparison to the microbead-based in situ assembled gratings, the microfabrication of grating enables commercializing, large area, and sensitive detection of biomolecular targets. In this study, we generated a NPL array of silica oxide by lithography and reactive ion etching (RIE) techniques as two-dimensional periodic relief gratings (2DPRGs) to increase the interface arising from protein adsorption to enhance the optical sensitivity. For one-dimensional periodic relief gratings (1DPRGs), the effective refractive indices for TM and TE polarization are perpendicular and parallel to the line patterns, respectively. The 1DPRG can be observed in solely pure color by the naked eye along the TM and TE directions. However, the observations by the naked eye along extremely precise TM or TE directions are very difficult so that 1DPRGs always display composed color images because colors of 1DPRG may vary sensitively with α and β angles (Figure 1).[20,22,23]

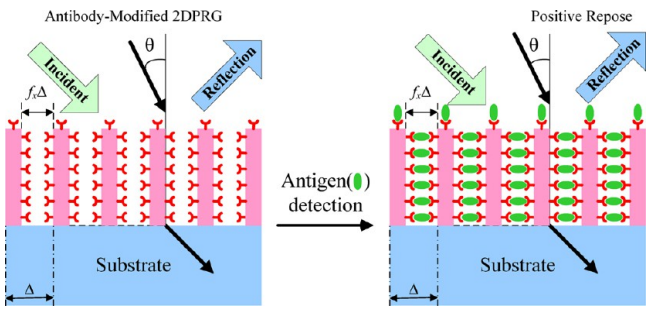

Figure 1. Schematic diagram of the sensor. A symmetric two-dimensional periodic relief grating (2DPRG) with filling factor. The effective refractive index from antigens attached to the antibody modified 2DPRG was observed by ellipsometry through illuminating the 2DPRG.

Comparing with 1DPRGs, colors of 2DPRGs observed by the naked eye are dependent solely on β angle, which can obtain better stability and chromatic aberration without issue of visual angles. Sequentially, antibodies were immobilized to the surface of the NPL array and used to capture the antigen from sample solutions changing the geometrical parameters and the refractive index of the gratings. Detection of the bound antigens was achieved by illuminating the surface with a visible light that diffracts due to the formation binding of the biological material. Specifically, an antigen-induced reformation mechanism in the 2DPRG system was shown to enable a large-scale morphological reorganization, resulting in refractive indices. This versatile process is particularly amenable to the creation of large-area uniform coatings on essentially any surface with precise control over the pillar scale of silicon oxide and optical properties of antibodies.

EXPERIMENTAL SECTION

Materials. Single-crystal Si wafers, Si(100), polished on one side (diameter: 6 in.) were supplied by Hitachi (Japan) and cut into 1.5 cm × 1.5 cm samples. The materials used for fabrication and characterization of antibody modified 2DPRG−3-aminopropyltriethoxysilane (APTES), tetraethoxysilane (TEOS), *N*-ethyl-*N*′-(3-dimethylaminopropyl) carbodiimide hydrochloride (EDC), bovine serum albumin (BSA), and *N*-hydroxysuccinimide (NHS) were purchased from Acros Organics and used as received without further purification. All other chemicals and solvents were of reagent grade and purchased from Aldrich Chemical. Purified recombinant protein G (proG) was purchased from Southern Biotech and reconstituted in phosphate buffered saline (10 mM). Purified mouse antihuman albumin (E-11; MAHA) and 3,3′,5,5′-tetramethylbenzidine (TMB) substrate buffer were purchased from Santa Cruz Biotechnology. Purified mouse HRP-human albumin (MHHA) was purchased from MyBioSource. Purified fluorescein (FITC)-conjugated AffiniPure goat antirabbit IgG (FGARI) was purchased from Jackson ImmunoResearch Lab.

Fabrication of Antibody-Modified 2DPRG. The basic strategy for the fabrication of the antibody-modified nanopillar array using the very-large-scale integration (VLSI) process and reactive ion etching (RIE) is depicted in Figure 2. (A) Deposition experiments were carried out by plasma-enhanced chemical vapor deposition (Oxford PECVD, 100 PECVD cassette system) with ca. 48 nm/min deposited rate. Oxygen was supplied through the same gas inlet with TEOS. Silicon oxide film was deposited on wafers with ca. 486 nm.[24] The Si wafer was treated with hexamethyldisilazane (HMDS) in a thermal evaporator (Track MK-8) at 90 °C for 30 s to transform the hydroxyl groups on the surface of wafer into an inert film of $Si(CH_3)_3$ groups for photoresist coating.[25] (B) Negative photoresist was spun on the HMDS-treated Si wafer at a thickness of ca. 360 nm. Advanced lithography was then used to pattern the photoresist with a nanopillar array possessing 200 nm scale after development. (C) Reactive-ion etching (Plasma Etcher, TEL TE5000) was used for the dry etching process after the photoresist was patterned onto the surface to cover the silicon oxide as a protection mask. Only the exposed regime of silicon dioxide was dry-etched by supplying a mixture gas of CHF_3 and CF_4 under the RIE process with 475.2 nm/min etching rate. The conditions are generally used for deep dry etch without any special surface requirements on solid state substrates. Sequentially, the remaining photoresist hard mask was removed from the surface by solvents, leaving behind a 2DPRG (nanopillar array) of silicon oxide. (D) The 2DPRG of silicon oxide was immersed in toluene solution possessing 1.5 wt % ATPES to assemble the amine groups on the surface.[26] (E) Commercially available recombinant protein G that minimizes nonspecific interactions with serum/cell proteins was covalently immobilized on the nanopillar surface by conjugation to the amine groups to give proG-2DPRGs. ProG guarantees an efficient orientation of the antibodies.[8,27] The amine groups on the surface of 2DPRG were activated by adding a solution of EDC and NHS. This mixture was allowed to shake for 90 min, diluted to 3 mL of PBS, and then 161 μL of proG (1 mg/mL) in PBS was added and the solution shaken for 3 h at 10 °C. The proG-modified 2DPRG was immediately cleaned ultrasonically for 90 min at 10 °C, the supernatant was decanted, PBS was added, and the cleaning process was repeated three more times to eliminate the excess of proG. Finally, the resulting

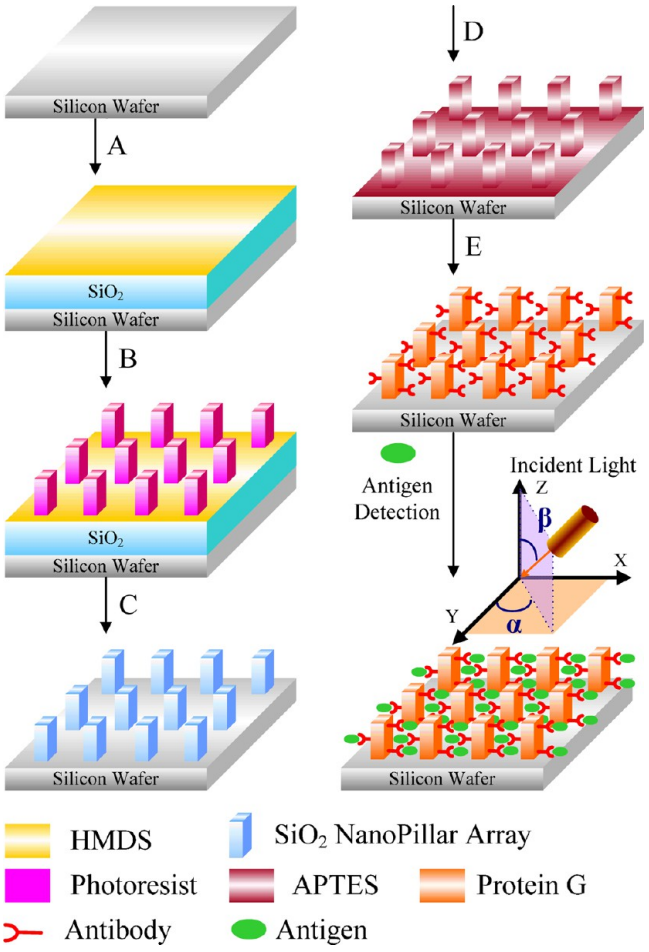

Figure 2. Schematic representation of the process used to fabricate MAHA-modified 2DPRG. (A) Silicon oxide film was deposited by plasma-enhanced chemical vapor deposition. The surface was treated with HMDS in a thermal evaporator. (B) A negative photoresist was spun on the HMDS-treated surface to pattern the photoresist as a 200 nm scale nanopillar array. (C) Only the exposed regime of silicon dioxide was dry-etched by supplying a mixture gas of CHF_3 and CF_4. Sequentially, the remaining photoresist hard mask was removed from the surface by solvents. (D) The 2DPRG of silicon oxide was treated with ATPES to assemble the amine groups. (E) The amine groups on the surface of 2DPRG were activated by adding a solution of EDC and NHS to immobilize proG on the pillar surface. MAHAs were oriented on the proG-modified pillar surface. The presence of MHHA could be detected by ellipsometry. Schematic representation of light traveling with α and β incident angle through a 2DPRG surface.

2DPRG is kept frozen until further use. Antibodies were then efficiently oriented onto the nanopillar surface by means of the immobilized proG, thus yielding a promising general platform for specific and sensitive detection of antigen by effective refractive index. A subject of proG-2DPRG conjugate was incubated for 6 h at 10 °C with 136 μL of MAHA in PBS buffer. The sample was cleaned ultrasonically for 90 min to separate any unbounded antibody, dissolved in PBS, and the cleaning process repeated until no antibody was recovered in the supernatant.

Characterization of Antibody Functionality by Immunocytostaining. Antibody concentrations immobilized on the pillar surface were determined by the Bradford protein assay through a FITC conjugated antibody—FGARI. After washing with PBS containing 0.05% Tween 20, the proG-modified 2DPRG was incubated with FGARI, and detected using an UV–vis spectrophotometer (Jasco, V-670). In addition, MAHA-modified 2DPRG and control 2DPRG without antibody modification were incubated with target MHHA and control BSA with various concentrations in PBS solution possessing 0.5% Tween 20 (pH 7.4, 10 mM) at 10 °C overnight. After washing at 4 °C for 90 min (three times), the presence of HRP-labeled antigen was determined by enzymatic-linked immunosorbent assay (ELISA) with TMB substrate buffer at 25 °C following the protocol supplied by Aldrich. After reaction, yellow solutions were measured at 450 nm, and the MHHA concentration was evaluated in the corresponding calibration curve. In addition, MAHA-modified 2DPRGs were analyzed using ellipsometry (SOPRA SE-5, France). The morphologies of the 2DPRG during selective immunosorbent assay were analyzed using an atomic force microscope (AFM; Veeco Dimension 5000 scanning probe microscope).

Optical Property of the 2DPRG during Immunosorbent Assay of Antigens. To be able to readily design and fabricate artificial dielectric elements, one must be able to relate the effective index to the grating profile in a simple way. By solution of Maxwell's equations with the relevant boundary conditions, the effective indices of one-dimensional (1D) and two-dimensional (2D) subwavelength gratings were obtained numerically by many authors.[28] Alternatively, the use of effective medium theory generally yields a good approximation if the period-to-wavelength ratio is sufficiently small. For 1D gratings, the theory gives simple expressions for the ordinary and extraordinary indices as follows:

$$n_{TE}^{\ 2} = f_1 n_1^{\ 2} + f_2 n_2^{\ 2} \quad (1)$$

$$n_{TM}^{\ -2} = f_1 n_1^{\ -2} + f_2 n_2^{\ -2} \quad (2)$$

where f_1 is the fill factor for medium 1 and $f_2 = 1 - f_1$ is the fill factor for medium 2. In the case of the 1D binary relief grating, the effective refractive indices for TE and TM polarizations are n_{TE} and n_{TM}, respectively. The different indices for the two polarization states indicate that 1D subwavelength gratings have form birefringence. Equations 1 and 2 are well-known results and have been frequently compared with rigorous calculations. The index in the direction normal to the grating vectors of a 2D subwavelength grating is given in effective-medium theory by

$$n_{eff} = [(1 - f_x f_y) n_1^{\ 2} + f_x f_y n_2^{\ 2}]^{1/2} \quad (3)$$

where f_x and f_y are the fill factors of medium 2 in the x and y directions, respectively (Figure 1). It has been noted that there are no simple closed-form zero-order expressions for the transverse principal effective indices of a 2D subwavelength grating. On the other hand, the indices can be bounded approximately by use of simple expressions derived from effective medium theory.[29] For simplicity, we will consider rectangular cylindrical geometries only. To set the upper bound, we view the 2D rectangular grating as a 1D grating consisting of strips lined up perpendicular to the electric field. Each strip in turn can be thought of as a section of a 1D grating with ridges parallel to the electric field. The effective index of each strip is calculated with eq 1. We then use these strip indices to calculate the overall effective index, using eq 2. This effective index is an upper bound that is exact in the static case and is given by

$$n_{eff,upper} = \left[\frac{1 - f_x}{n_1^{\ 2}} + \frac{f_x}{f_y n_2^{\ 2} + (1 - f_y) n_1^{\ 2}} \right]^{-1/2} \quad (4)$$

To obtain the lower bound, we view the 2D grating as a 1D grating consisting of strips parallel to the electric field. The effective index of each strip is now found by use of eq 2, and the overall effective index, representing the lower bound, by use of eq 1, giving

$$n_{eff,lower} = \left[(1 - f_y) n_1^{\ 2} + \frac{f_y}{f_x n_2^{\ -2} + (1 - f_x) n_1^{\ -2}} \right]^{1/2} \quad (5)$$

We obtain the effective-index bounds in the y direction by interchanging the x and y subscripts. At all times, the bounds lie between the indices of the two components of the artificial dielectric.

RESULTS AND DISCUSSION

Characterization of the MAHA-Modified 2DPRG. The free amine group of the 2DPRG directs covalent conjugation of commercially available proG by carboxyl group coupling. ATPES-modified 2DPRGs were first activated with EDC/NHS and immersed in PBS (pH 7.4) in the presence of 1, 3, or 5 equiv of proG. An excess of proG was recovered by using 5 equiv of proG, securing that the maximum number of amine groups are coupled to the protein. The random covalent binding of proG does not represent a problem, as this molecule presents several immunoglobulin G binding sites.[30] The oriented capture of antibodies by proG has been shown to be superior for retaining their activity versus the disordered orientation of MAHA molecules obtained by direct functionalization onto the surface.[31] ProG-modified 2DPRG was incubated with FGARI in Tris/glycine buffer, pH 9, for 6 h at 10 °C. The conjugates were cleaned until the washings did not show any free FGARI. To confirm the presence of the FGARI on the 2DPRGs, a Bradford assay experiment was carried out. The amount of FGARI present on the 2DPRG was also estimated by quantifying the amount of recovered FGARI in the supernatant after washing by the Bradford method.[32] The peak of FGARI present on the pillar surface was clearly visible at 595 nm, which corresponds to the specific peak of FITC. The result indicates that the concentration of antibody molecules was ca. 1.64 mg/m^2. Apart from the amount of antibody conjugated to the proG-modified 2DPRGs, it was critical to assess the biofunctionality of the antibodies on the nanopillar surface. As a first proof of principle of the sensing potential of our MAHA-conjugated 2DPRGs, a monoclonal MAHA was conjugated to the proG-2DPRGs, and immunosorbent assay of the HRP-labeled antigen (MHHA) was performed. The MHHA and free BSA as a control were enzyme-linked directly with the MAHA-modified 2DPRGs. In order to quantify antibody activity, an immunoassay was performed where a MAHA was coupled to the proG-modified 2DPRG and a MHHA was chosen as a target antibody. As a control experiment, 2DPRGs without proG treatment were also submitted to the immunoassay. MHHA is recognized only by well oriented MAHA. The oxidation of TMB catalyzed by horseradish peroxidase (HRP) enzyme was evaluated by the absorbance at 450 nm (Figure 3a). The different absorbance intensities obtained for the MAHA and MAHA-proG modified 2DPRG experiments with MHHA revealed that 72% of the secondary mAb was recognized by the MAHA-proG modified 2DPRG, indicating the coupling efficiency of the oriented MAHA on the surface. In addition, the MHHA concentrations immobilized on the pillar surface inside 2DPRG through coupling with MAHA were calculated with various coupling times, as shown in Figure 3b. The surface concentrations of MHHA coupled with MAHA on the pillar surface increased with coupling times upon 6 min, indicating that the saturated surface concentration of antigen molecules inside the 2DPRG was ca. 3.51 mg/m^2.

Morphology Change of MAHA-Modified 2DPRG during Selective Immunosorbent Assay. When the antibody-modified 2DPRG couples specifically with target antigen, the geometrical parameters of the 2DPRGs and/or the refractive index contrast typically change. According to the effective-medium theory, the fill factors in the x directions (f_x) and y direction (f_y) represent the pillar scales (Figure 2). Atomic force microscopy (AFM) was used to visualize the

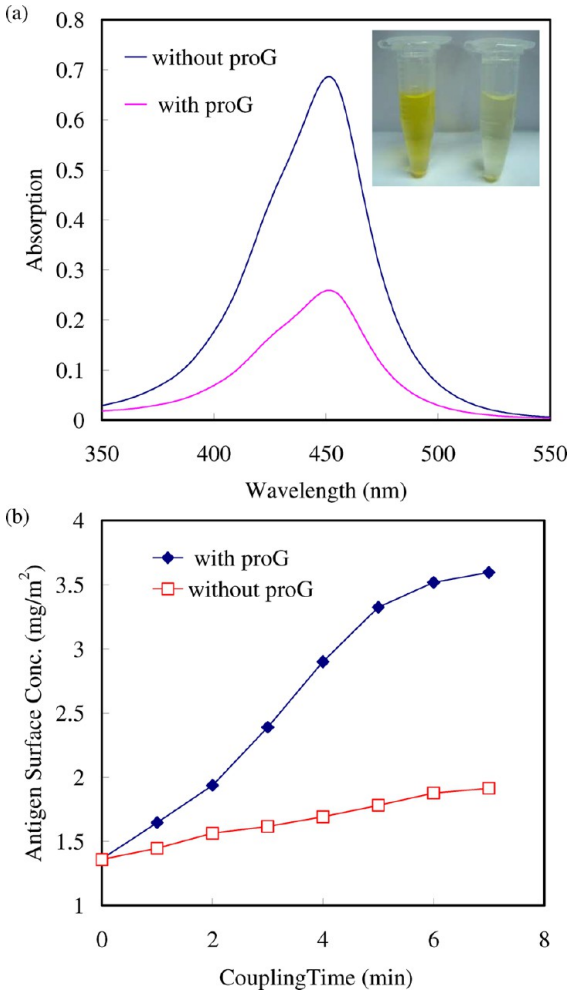

Figure 3. (a) UV−vis spectra of ELISA for the MAHA-modified 2DPRG with and without proG treatment. Photographic images demonstrate the color change of target antigen (MHHA) by MAHA conjugate with (left) and without (right) proG treatment was estimated after washing in terms of HRP enzymatic activity. (b) MHHA surface concentration in the 2DPRG plotted with respect to coupling time with MAHA on the pillar surface.

morphology of the antibody-modified 2DPRG. 3D (left), 2D, and line cross-section (right) analysis AFM topographic images of the MAHA-modified 2DPRG were depicted in Figure 3a, revealing that the MAHA-modified 2DPRG on the Si surface existed as a dense distinctive overlayer, with pillar scales of ca. 215 nm, within a scanning area of 10 × 10 μm^2. From line cross-section analysis, the pillar array texture was clearly shown. Each pillar of the antibody-modified 2DPRG was fabricated successfully in a regular array with a similar height of 438 ± 3 nm. The 2DPRG consisted of a repeating pattern of 231 ± 3 nm pillars and 164 ± 3 nm spaces over a large area. The period of this grating was controlled below the wavelength used to enhance the grating effect. The scales of proG and antibody are ca. 2 and 13.1 nm, respectively, corresponding to the pillar scale increase and space decrease. MAHA bound to the pillar surface remains able to recognize and bind their antigen efficiently and specifically. The silicon surfaces are then washed in PBS solution after the target antigens are allowed to bind to the antibody, and the complexes remain bound to the 2DPRG. 3D (left), 2D, and line cross-section (right) analysis AFM topographic images of the antibody-modified 2DPRG after

dx.doi.org/10.1021/am4004123 | ACS Appl. Mater. Interfaces 2013, 5, 3348−3355

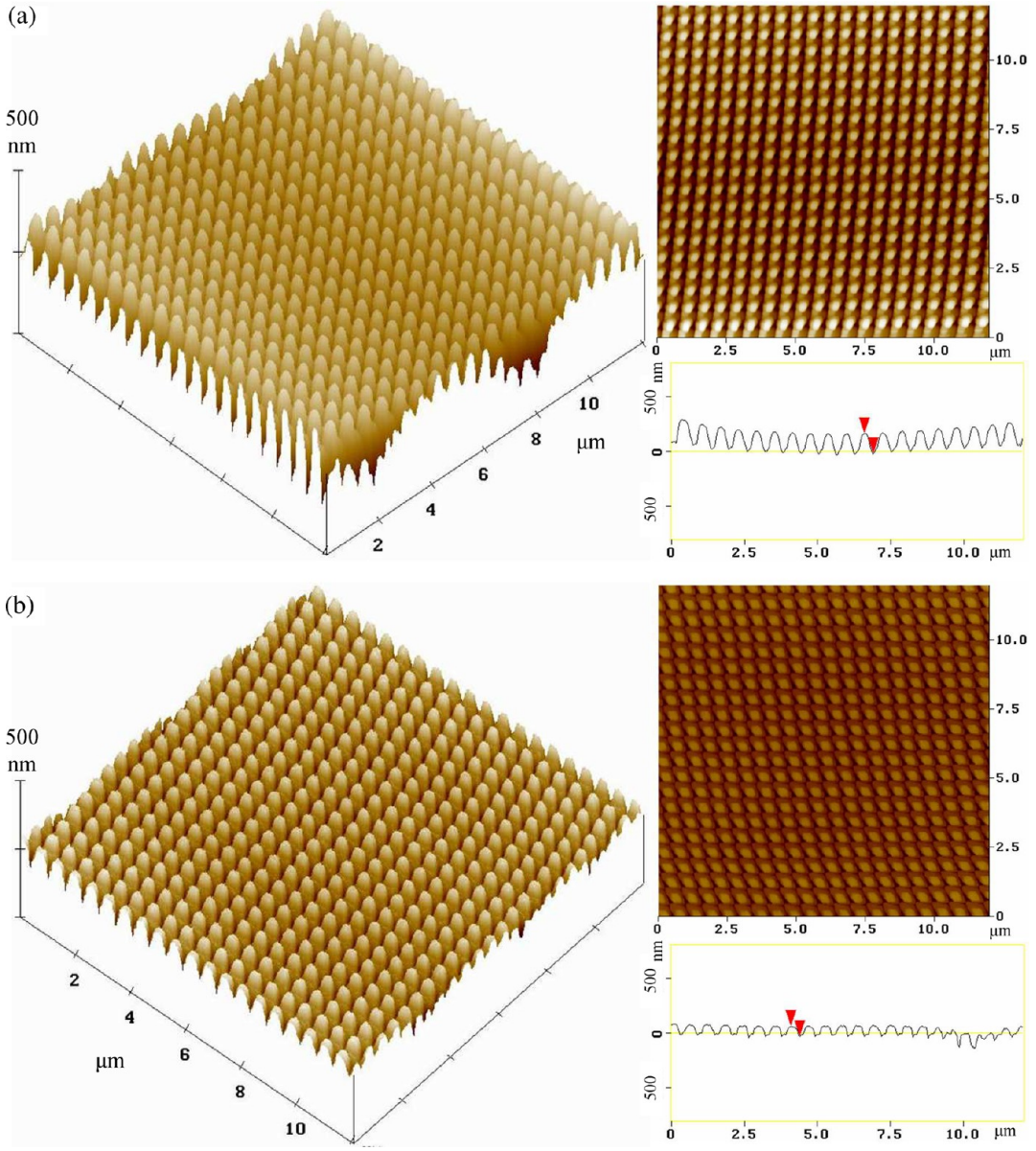

Figure 4. 3D (left), 2D (right), and line cross-section (right) analysis AFM topographic images of the MAHA-modified 2DPRG (a) before and (b) after MHHA coupling.

bonding target antigens were depicted in Figure 3b. As a result, the regular pillar array remained obviously after target antigen binding. The scale of each pillar was increased obviously from 231 ± 3 to 315 ± 3 nm and space of 80 ± 4 nm. In addition, the height of each pillar dramatically changed from 438 ± 3 to 217 ± 3 nm. The results suggest that the antigens may aggregate on the pillar bottom, which could not be readily removed from the nanostructure by the washing process. Note that ridges observed in the 3D AFM image of Figure 4a did not appear in the 2D AFM image, implying the inaccuracy of fist scratching during AFM measurement. To verify that the MHHA were bound only to MAHA-modified areas, BSAs were allowed to bind to the surfaces. The silicon surfaces are then washed in PBS solution possessing 0.5% Tween 20 (pH 7.4, 10 mM) at 10 °C after BSA immersion to reduce nonspecific binding by the inclusion of Tween into the buffer. No apparent variation in the geometrical parameters over the entire sample area is a result of a specific binding, thus confirming the functionality and specificity of the antigens after capture by protG-2DPRGs. The amount of nonspecific interactions was negligible, as indicated by the control experiments. Despite these variations of geometrical parameters, these samples effectively bound MHHA as measured by effective refractive index.

Characterization of Selective Immunosorbent Assay in Optical Properties. We measured the refractive index of MHHA thin film at 632.8 nm in a result of 1.4374, closed to the previous reports,[33] as a standard value by ellipsometry. Further characterization of MHHA attached to the MAHA-modified 2DPRG was obtained using the effective refractive index (n_{eff}) obtained from ellipsometry. Figure 5 shows the n_{eff} of bare 2DPRG (A), proG-2DPRG (B), and antibody-proG-2DPRG (C) obtained by environmental ellipsometry at 633 nm wavelength. The refractive index of MHHA is close to that of silicon oxide (1.46), regarded as the same component in effective medium theory. The dramatic response in n_{eff} occurs

dx.doi.org/10.1021/am4004123 | ACS Appl. Mater. Interfaces 2013, 5, 3348−3355

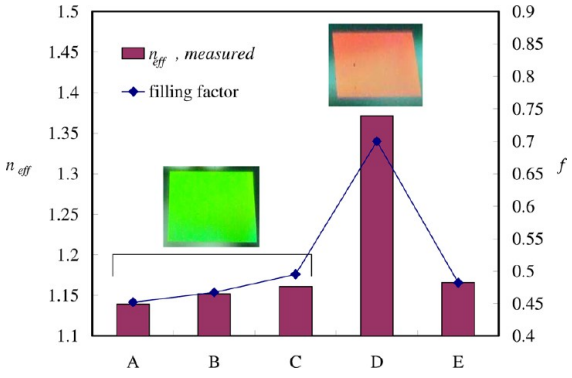

Figure 5. n_{eff}, measured using ellipsometry, of bare 2DPRG (A), proG-2DPRG (B), MAHA modified 2DPRG (C), MAHA modified 2DPRG after MHHA coupling (D), and MAHA-modified 2DPRG after control BSA binding (E). Photographic images for A–C and D demonstrate the grating effect of the 2DPRG.

specifically after MHHA coupling with MAHA on the pillar surface, probed by ellipsometry (D in Figure 5). In addition, the n_{eff} remained a similar value as well as MAHA-modified 2DPRG after control BSA immersing, indicating the BSA did not significantly couple with the MAHA on the pillar surface (E in Figure 5). Photographic images of the MAHA-modified 2DPRG before and after antigen coupling, obtained at a β angle of ca. 10–20° (Figure 2), are inserted in Figure 5. The 2DPRG was prepared into a die using an etching process with a 1 cm × 1 cm contact mask. The light impinging the sample at an incident angle is linearly polarized, with the electric-field vibration parallel p or perpendicular s to the plane of incidence. The reflected light will also be p- or s-polarized. In this work, we observe the reflection of the 2DPRG by the naked eye under an invariable β angle.[34] At a β angle close to 10–20°, the antibody modified 2DPRG displays pure green color before MHHA coupling. The color turns obviously to orange color instead of the initial green color after MHHA coupling. The visualized color changes are provided to detect specific antigen rapidly and conveniently. The effect of diffractive grating is dependent on the period and/or the angle of observation when the structure scale of a grating is larger than the wavelength. Therefore, the period and angle of observation are fixed possibly in our case. Furthermore, the scale of each pillar of 2DPRG is 200 nm less than the wavelength; it may not follow the diffraction grating theory, filling factor do not affect the color change of the grating.

Figure 6a displays the sensitivity of the MAHA-modified 2DPRG under MHHA coupling through n_{eff} for 5 min in terms of MHHA concentrations. The pillar scale variation appears to occur over the antigen concentration range 0.2–1.6 μg/mL for 5 min, with the majority of the variation between 0.6 and 1.0 μg/mL, defined as a detection limit of concentration within a period of time. The results indicate that the quantity of MHHA coupled with MAHA-modified 2DPRG increases upon 0.6 μg/mL of MHHA during the period. The quantity of MHHA coupled on the pillars may not be sufficient to generate significant change in filling factor and n_{eff} of 2DDPRG for 5 min when its concentration is below 0.6 μg/mL. If the sample is immersed in 0.6 μg/mL MHHA solution for sufficient time, such as 30 min, the filling factor and n_{eff} change significantly. However, we expect the sample could respond within 5 min during immunosorbent assay. We observe approximately linear increases in n_{eff} of the 2DPRG from 0.6 μg/mL, indicating the

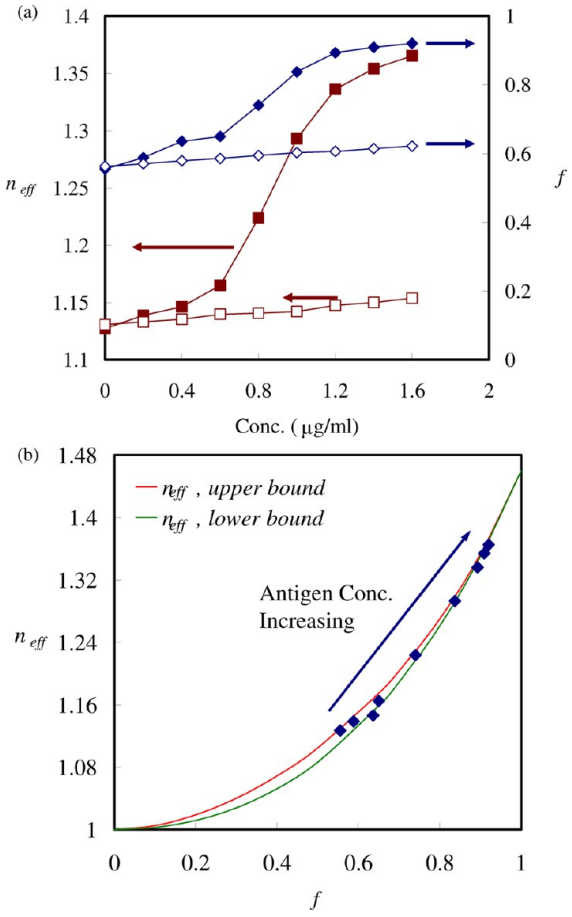

Figure 6. (a) Changes in n_{eff} and f of the 2DPRG plotted as a function of MHHA concentration in the solution. (b) n_{eff} of 2DPRG plotted as a function of f with increasing MHHA concentration in the solution, fitted to eqs 7 and 8.

detection limit of MHHA concentration. The results suggest that n_{eff} of the 2DPRG was related substantially with changes in the degree of specific antigen coupling and a concomitant change in the filling degree of the 2DPRG within the period.

A 2DPRG is regarded that an air layer is filled by silicon oxide with antigen; n_1 and n_2 are represented by air and silicon oxide with antigen in eq 3, respectively. For the convenience, the fill factors in the x directions (f_x) are set to be equal to that in the y direction (f_y) for description of the square pillar structure. Equations 3, 4, and 5 could be rewritten as eqs 6, 7, and 8 in the following, respectively.

$$n_{eff} = [(1 - f^2)n_1^2 + f^2 n_2^2]^{1/2} \quad (6)$$

$$n_{eff,upper} = \left[\frac{1 - f}{n_1^2} + \frac{f}{fn_2^2 + (1 - f)n_1^2}\right]^{-1/2} \quad (7)$$

$$n_{eff,lower} = \left[(1 - f)n_1^2 + \frac{f}{fn_2^{-2} + (1 - f)n_1^{-2}}\right]^{-1/2} \quad (8)$$

We calculated f by using the measured n_{eff}, calculated by pillar scale change during antigen coupling processes. The effective medium theory certainly obtains a much more accurate result only when the period is sufficiently smaller than the wavelength. Therefore, we use the bounded indices expressions to fit our results. The report suggests that the effective indices

dx.doi.org/10.1021/am4004123 | ACS Appl. Mater. Interfaces 2013, 5, 3348–3355

are on average increased by at most 3% for a 2D 400 nm period symmetric grating at a wavelength of 633 nm.[35] The inaccuracy of refractive indices for 200 nm scale 2DPRG at a wavelength of 633 nm may be on average less than 3%. Figure 6a presents the dependence of calculated f of the 2DPRG by eq 6 with the antigen concentrations during the coupling process. The results suggest that the MAHA-modified 2DPRG featured increasing the filling volume of the antigen surrounding the pillar structure. Moreover, these n_{eff} and f varied with antigen concentrations are evaluated by the eqs 7 and 8 model in the effective medium theory. The eqs 7 and 8 model for n_{eff} and f were constructed to fit only data at 633 nm to avoid lower wavelength regions which are strongly absorbed by the surface coverslip, as shown in Figure 6b. The measured n_{eff} located inside the region bounded by eqs 7 and 8 with an increase of MHHA concentration could be regarded as a close fit; even the refractive indices of silicon oxide and MHHA are assumed to be equal. The upward concaves specifically represent the n_{eff} exhibited in the 2D pillar SWSs as a function of filling factors, consistent with the pervious report.[33,35] The model perfectly matched the measured data in various antigen concentrations during the MHHA coupling process. The results indicate that the inherent sensitivity based on measurements on detecting the change of refractive index by ellipsometry across the interface arising from protein adsorption can be enhanced through a 2DPRG structure. Moreover, other 2DPRGs with various scales are fabricated to investigate the sensitivity of the antigen coupling. A direct measure of the bound MHHA on the MAHA modified 2DPRG was obtained by measuring the n_{eff}. The color effect present with the antigens attached to the antibody modified 2DPRG could easily be seen by the naked eye when the pillar scale of 2DPRG is less than 600 nm. A linear relationship between the detection limit of antigen concentration and the pillar scale is observed (Figure 7). The

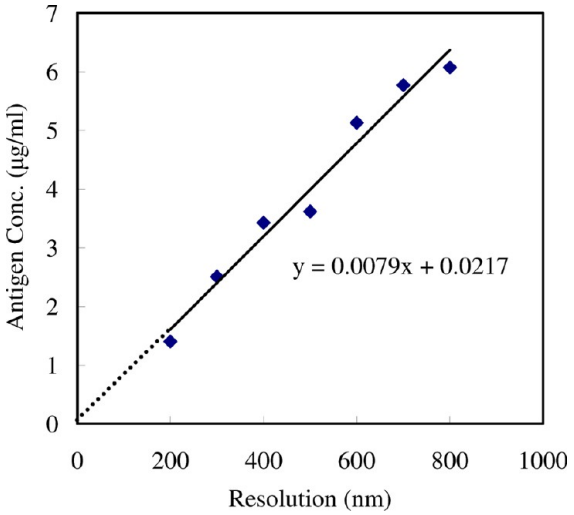

Figure 7. Dependence of the detection limit of MHHA concentration with the nanopillar scale of 2DPRG.

detection limit of antigen concentration increased linearly with the pillar scale upon 800 nm. This plot was generated by taking the n_{eff} measurements of MAHA-modified samples to obtain a background reading for each antigen concentration. Downward extending the linear relationship, the detect limit of antigen concentration may be approached to ca. 0.4 μg/mL for a 50 nm scale 2DPRG. In the present study, we have generated a 2DPRG as a platform of selective immunosorbent assay. The detection approach is established because only antigen is bound to the antibody modified region. The color effect observed when illuminating the nanometer-scale grating is most likely due to the effective refractive index difference during antigen coupling.

CONCLUSIONS

Recently, more elaborate methods of directing antibodies to surfaces have been achieved using diffractive grating. We have substantially modified a specific antibody on the pillar surface of 200 nm scale 2DPRG on a large area capable of antigen detection. By selecting a suitably functional antibody and optimizing the coupling process with antigen, the scale of the nanostructures could be readily altered. Although we cannot exclude any desorption of the antigens after coupling with antibodies, the filling behavior of antigens among the pillars is sufficiently robust to survive the subsequent process and yield a consistent, detectable signal of effective refractive index. 2DPRG is a simple structure to generate an immunoreactive nanostructured surface that eliminates any prior treatment and complications. The effective refractive index measurements are not susceptible to small defects; therefore, any nonuniformities resulting from the fabrication process are not critical to the measurements. Although there are opportunities to improve the surface plasmon resonance to generate optical biosensors, the current format presented in this study appears to be effective. Moreover, the light impinging the 2DPRG at an incident angle of 10−20° displays the pure green and orange color observed by the naked eye before and after antigen binding, respectively. This simple sensor may have apparent color change in the antigen detection as well as any cell with specific antigen whose volume is sufficient to fill in the pillar structure when bound on a silicon surface.

AUTHOR INFORMATION

Corresponding Author

*Phone: +886-2-27376523. Fax: +886-2-27376544. E-mail: jkchen@mail.ntust.edu.tw.

Notes

The authors declare no competing financial interest.

ACKNOWLEDGMENTS

We thank the National Science Council of the Republic of China for supporting this research financially and the National Nano Device Laboratory for assistance with the electron beam lithography and RIE, respectively.

REFERENCES

(1) Wu, G. H.; Datar, R. H.; Hansen, K. M.; Thundat, T.; Cote, R. J.; Majumdar, A. *Nat. Biotechnol.* **2001**, *19*, 856−860.
(2) Kim, S. J.; Gobi, K. V.; Tanaka, H.; Shoyama, Y.; Miura, N. *Chem. Lett.* **2006**, *35*, 1132−1133.
(3) Henne, W. A.; Doorneweerd, D. D.; Lee, J.; Low, P. S.; Savran, C. *Anal. Chem.* **2006**, *78*, 4880−4884.
(4) Jenison, R.; Yang, S.; Haeberli, A.; Polisky, B. *Nat. Biotechnol.* **2001**, *19*, 62−65.
(5) Goh, J. B.; Tam, P. L.; Loo, R. W.; Goh, M. C. *Anal. Biochem.* **2003**, *313*, 262−266.
(6) Zhao, W.; Zhang, W.-P.; Zhang, Z.-L.; He, R.-L.; Lin, Y.; Xie, M.; Wang, H.-Z.; Pang, D.-W. *Anal. Chem.* **2012**, *84*, 2358−2365.
(7) García, I.; Gallo, J.; Genicio, N.; Padro, D.; Penadés, S. *Bioconjugate Chem.* **2011**, *22*, 264−273.

(8) Lee, J. Y.; Mai, L. W.; Hsu, C. C.; Sung, Y. Y. *Opt. Commun.* **2012**, *289*, 28−32.
(9) Jeong, H. H.; Erdene, N.; Park, J. H.; Jeong, D. H.; Lee, H. Y.; Lee, S. K. *Biosens. Bioelectron.* **2013**, *39*, 346−351.
(10) Mohan, K. D.; Oldenburg, A. L. *Opt. Express* **2012**, *20*, 18887−18897.
(11) Sainz-Gonzalo, F. J.; Elosua, C.; Fernandez-Sanchez, J. F.; Popovici, C.; Fernandez, I.; Ortiz, F. L.; Arregui, F. J.; Matias, I. R.; Fernandez-Gutierrez, A. *Sens. Actuators, B* **2012**, *173*, 254−261.
(12) St. John, P. M.; Davis, R.; Cady, N.; Czajka, J.; Batt, C. A.; Craighead, H. G. *Anal. Chem.* **1998**, *70*, 1108−1111.
(13) Neubert, H.; Jacoby, E. S.; Bansal, S. S.; Iles, R. K.; Cowan, D. A.; Kicman, A. T. *Anal. Chem.* **2002**, *74*, 3677−3683.
(14) Yeh, W.; Kleingartner, J.; Hillier, A. C. *Anal. Chem.* **2010**, *82* (12), 4988−4993.
(15) Szabó, Z.; Volk, J.; Fülöp, E.; Deák, A.; Bársony, I. *Photonics Nanostruct.* **2013**, *11*, 1−7.
(16) Zhang, Y.; Lo, C.-W.; Taylor, J. A.; Yang, S. *Langmuir* **2006**, *22* (20), 8595−8601.
(17) Hirade, M.; Nakanotani, H.; Yahiro, M.; Adachi, C. *ACS Appl. Mater. Interfaces* **2011**, *3* (1), 80−83.
(18) Chen, J.-K.; Wang, J.-H.; Fan, S.-K.; Chang, J.-Y. *J. Phys. Chem. C* **2012**, *116*, 6980−6992.
(19) Saito, M.; Kitamura, A.; Murahashi, M.; Yamanaka, K.; Hoa, L.; Yamaguchi, Y.; Tamiya, E. *Anal. Chem.* **2012**, *84* (13), 5494−5500.
(20) Ye, G.; Wang, X. *Biosens. Bioelectron.* **2010**, *26*, 772−777.
(21) Chang, C. L.; Acharya, G.; Savran, C. A. *Appl. Phys. Lett.* **2007**, 90.
(22) Chen, J. K.; Bai, B. J. *J. Phys. Chem. C* **2011**, *115*, 21341−21350.
(23) Chen, J.-K.; Pai, P.-C.; Chang, J.-Y.; Fan, S.-K. *ACS Appl. Mater. Interfaces* **2012**, *4*, 1935−1947.
(24) Dinga, Y.; Pana, Q.; Jina, J.; Jiab, H.; Shirai, H. *Thin Solid Films* **2010**, *518*, 3487−3491.
(25) Chen, J. K.; Zhuang, A.-L. *J. Phys. Chem. C* **2010**, *114*, 11801−11809.
(26) Chen, J. K.; Hsieh, C. Y.; Huang, C. F.; Li, P. M.; Kuo, S. W.; Chang, F. C. *Macromolecules* **2008**, *41*, 8729−8736.
(27) Lee, J. M.; Park, H. K.; Jung, Y.; Kim, J. K.; Jung, S. O.; Chung, B. H. *Anal. Chem.* **2007**, 79−2687.
(28) Grann, E. B.; Moharam, M. G..; Pommet, D. A. *J. Opt. Soc. Am. A* **1994**, *11*, 2695.
(29) Jackson, J. L.; Coriell, S. R. *J. Appl. Phys.* **1968**, *39*, 2349.
(30) Akerström, B.; Björtck, L. *J. Biol. Chem.* **1986**, *261*, 10240−10247.
(31) Jung, Y.; Lee, J.; Jung, H.; Chung, B. *Anal. Chem.* **2007**, *79* (17), 6534−6541.
(32) Bradford, M. M. *Anal. Biochem.* **1976**, *72*, 248−254.
(33) Kikuta, H.; Toyota, H.; Yui, W. *Opt. Rev.* **2003**, *10*, 63−73.
(34) Burton, Z.; Bhushan, B. *Nano Lett.* **2005**, *5* (8), 1607−1613.
(35) Chen, F. T.; Craighead, H. G. *Opt. Lett.* **1995**, *20* (2), 121−123.